Research Article

Shiqi Fan[#], Zhen Tan[#], Zhiyu Peng, Shilei Li, Haoyuan Lei, Yuxiang Qin, Hongyuan Fan, Yuanhua Lin*, and Changchun Zhou

Customized 3D printed porous titanium scaffolds with nanotubes loading antibacterial drugs for bone tissue engineering

https://doi.org/10.1515/rams-2024-0030 received December 13, 2023; accepted May 14, 2024

Abstract: Due to the uncertainty of trauma or infection, customized bone substitutes are often required in clinic. Meanwhile, excessive use of antibiotics may lead to drug resistance. Therefore, the design of anti-infection bone tissue engineering scaffold is of very important. In this study, porous titanium alloy bone tissue engineering scaffolds were designed and fabricated by 3D printing. TiO2 nanotubes were further constructed on the scaffolds through electrochemical anodic oxidation, achieving the drug loading and anti-infection functions. The micron-level bionic pores were fabricated by the 3D printing process, and the secondary nanoscale-level nanotubes were achieved through the anodic oxidation process. Thereafter, the micro-nano structured porous bone tissue engineering scaffolds are presented. This structure features that the drug release rate can be regulated by loading the anti-infection drug minocycline

These authors contributed equally to this work and should be considered first co-authors.

* Corresponding author: Yuanhua Lin, School of New Energy and Materials, Southwest Petroleum University, Chengdu, 610500, China; State Key Laboratory of Oil and Gas Reservoir Geology and Exploitation, Southwest Petroleum University, Chengdu, 610500, China, e-mail: Yhlin28@163.com

e-mail. militz8@105.com

Shiqi Fan: School of New Energy and Materials, Southwest Petroleum University, Chengdu, 610500, China

Zhen Tan: Department of Bone and Joint Surgery, Peking University Shenzhen Hospital, Shenzhen, 518036, China; School of New Energy and Materials, Southwest Petroleum University, Chengdu, 610500, China Zhiyu Peng: Department of Thoracic Surgery, West China School of Medicine, West China Hospital, Sichuan University, Chengdu, 610041, China

Shilei Li, Hongyuan Fan: School of Mechanical Engineering, Sichuan University, Chengdu, 610065, China

Haoyuan Lei, Yuxiang Qin, Changchun Zhou: National Engineering Research Center for Biomaterials, School of Biomedical Engineering, Sichuan University, Chengdu, 610064, China

and coating them with poly(lactic-co-glycolic acid) (PLGA) in the nanotubes. According to the results, the micro–nano composite porous scaffold showed uniform and controllable micro–nano pores, it may load anti-infection drugs and shown anti-infection ability. In addition, the PLGA coating may delay the drug release and maintain a sustained anti-infection function for the scaffold in a week. This study provides new ideas for designing antibacterial bone tissue engineering scaffold.

Keywords: 3D printing, Ti6Al4V scaffolds, electrodeposition, nanotubes, anti-infection function

1 Introduction

Now the world is seeing an increasing number of scaffold surgeries year by year, which poses a great challenge to the traditional scaffold industry [1]. Due to individual differences between patients, there are different requirements for scaffolds, including scaffold shape and size. An ideal bone tissue scaffold should have the similar structure and mechanical properties with native bones [2-4]. Scaffolds with a suitable 3D porous structure and excellent surface bioactivity are regarded as ideal bone tissue scaffolds. After a scaffold is embedded into body, interconnected pores can serve as channels for the transfer of nutrients and the discharge of metabolic waste [5,6]. Selective laser melting (SLM) is an additive manufacturing technology. It instantaneously melts and solidifies metal powder using laser along designed paths to form the desired parts [7-10]. SLM technology has been widely used in biomedicine and aerospace fields because of its high forming precision and complex structure forming.

Titanium and its alloys have been used as bone scaffolds for decades largely due to their corrosion resistance and appropriate biomechanical properties [11–16]. Bone scaffolds not only provide mechanical support and function but also serve as the matrix for the interactions among various proteins and cells. These interactions determine the degree of bone integration and the healing velocity of bones around a scaffold. Titanium alloy is biologically inert and difficult to connect directly with human bone tissue, which may loosen the scaffold or even cause a surgical failure. For the above reason, as the first part of contact with the surrounding tissue, the surface of scaffold plays an important role in determining the future of scaffolds. Anodic oxidation is a surface treatment method suitable for titanium alloy. According to the findings of many studies, anodic oxidation generates regular nanomorphology, also known as nanotubes. Nanotubes can enhance the bioactivity of scaffolds, improve cell adhesion and proliferation, and reduce bacterial adhesion [17-21]. Different from other surface treatment methods, anodic oxidation preserves the internal biomechanical stability of titanium alloy scaffolds. With a tubular shape, nanotubes have great potential for drug loading [22,23].

Minocycline (MH) is one of the tetracycline antibiotics with a broad spectrum of anti-infection effects, including gram-positive and gram-negative bacteria, anaerobic bacteria, rickettsia, and mycoplasma. When bone replacement surgeries are performed, there is a risk of bacterial infection at the surgical site. MH, being effective against a wide range of bacteria, can help prevent and treat such infections. As for the mechanism of action, MH inhibits bacterial protein synthesis and prevents aminoacyl-tRNA binding during bacterial translation in particular. Besides, MH can suppress the activity of collagenase, succinic dehydrogenase, thrombin, and some other enzymes, thereby protecting against inflammation and tissue damage. Controlling inflammation at the surgical site is crucial for the proper healing of bones after replacement. MH can help modulate the inflammatory response, supporting the overall healing process. PLGA is the abbreviation of poly (lactic-co-glycolic acid) and is a kind of biodegradable polymer. It is composed of the copolymer of lactic acid and glycolic acid, and therefore has complex polymer structures. It has been widely used in the fields of medicine and biotechnology [24,25]. PLGA can be tailored to achieve controlled drug release. The polymer degrades over time, releasing the encapsulated drug gradually. This controlled release profile is crucial in maintaining therapeutic drug concentrations at the site of action, optimizing treatment efficacy while minimizing potential side effects. PLGA is compatible with a wide range of drugs, including antibiotics like MH. This allows for the encapsulation of MH within PLGA particles or coatings, facilitating its controlled release at the bone replacement site.

In this study, we proposed a method to enhance the anti-infection function of titanium alloy scaffolds by 3D printing (additive manufacturing) and surface modification. The research ideas and experimental methods of

this study are shown in Figure 1. In this study, the Solidworks software was used to design micron-level porous scaffold models and then output the models for SLM 3D printer. After acid treatment, a layer of nano-scale pores was constructed on the surface by electrochemical anodic oxidation, so that the scaffolds have a composite structure in both micron scale and nano-scale. In the process of anodic oxidation, the appearance of nanotubes is regulated by changing the anodic oxidation voltage and anodic oxidation time, and the scaffold appearance is analyzed by X-ray diffraction (XRD) and scanning electron microscope (SEM) to ensure the drug loading potential of nanotubes. MH is then loaded into nanotubes and the nanotubes are finally encapsulated using PLGA through physical cycling [26,27]. The biological properties of the anti-infection scaffolds are evaluated in terms of drug release, cytotoxicity, and bacterial adhesion.

2 Materials and methods

2.1 Design and 3D printing of porous titanium alloy scaffolds

The porous titanium alloy scaffolds were designed by means of Solidworks. Literature suggests that the ideal pore size of a bone tissue engineering scaffold is 300–900 μm and ideal porosity ranges within 60–95% [28]. Thereafter, as shown in Figure 2, a diamond structure with pores of 660 μm and struts diameter of 330 μm was used as the basic pore unit of the scaffold, and the scaffold's shape was a cylinder with a height of 5 mm and diameter of 10 mm ($\Phi 10 \times 5$ mm). This structure has good load bearing capacity and can smoothly conduct stress to maintain the integrity of the structure and function [29]. The scaffolds were made by SLM system (M2, Concept laser, German). The selected Ti6Al4V powder with diameter of 17–50 μm was used as the printing raw materials. The printer had a laser power of 90 W and the laser scanning speed was set to 500 mm·s $^{-1}$.

2.2 Surface modification and characterization of the porous titanium alloy scaffolds

The residual printing powder on the porous scaffolds was first removed by chemical corrosion (pickling) [30]. The corrosive solution was hydrofluoric acid (HF) solution consisting of 1 mL HF (40.0 wt%, Chengdu Chron Chemical Reagent Factory, Sichuan, China) and 50 mL deionized

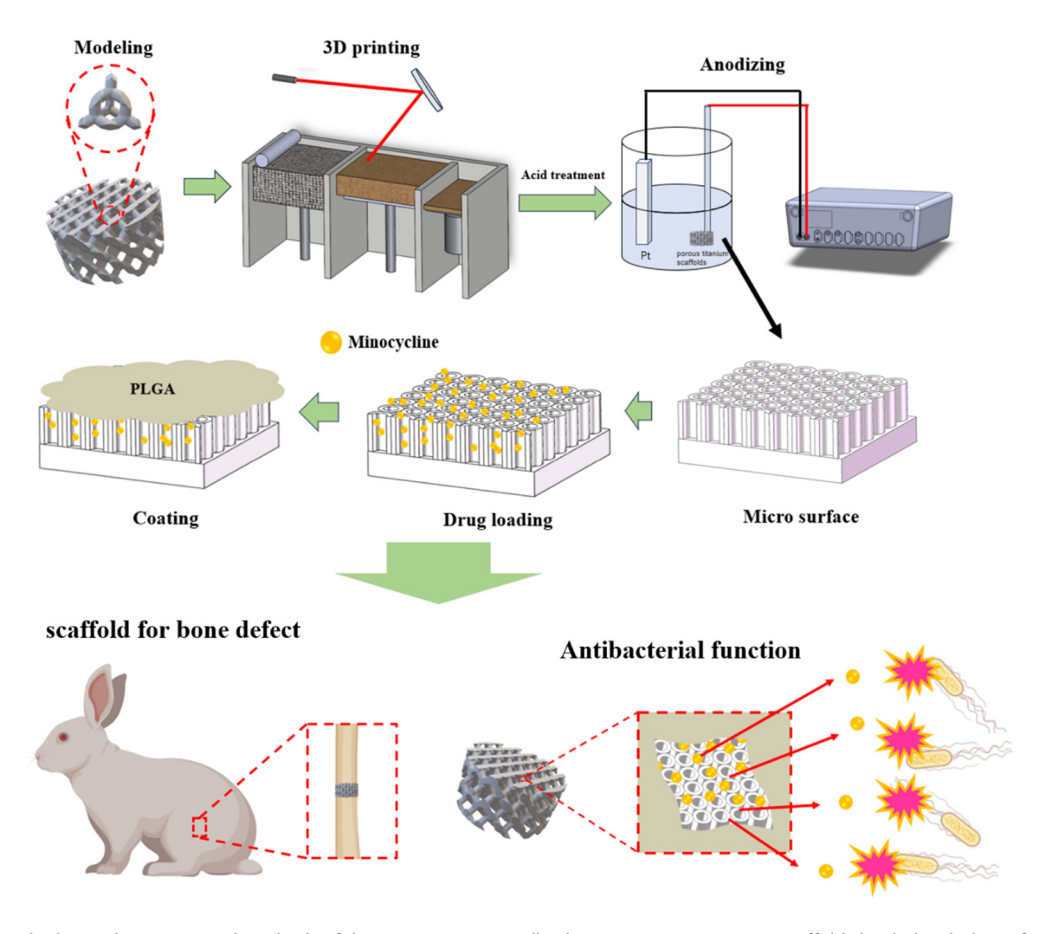


Figure 1: Research idea and experimental methods of the porous titanium alloy bone tissue engineering scaffolds loaded with drugs for anti-infection function application.

water. The scaffolds were put into the corrosive solution for 15 min of reaction at room temperature. Then the corroded samples were put into deionized water and treated by ultrasonic waves for 5 min. This process was repeated three times. After being washed with deionized water, the scaffolds were put into absolute alcohol and then treated by ultrasonic waves for 5 min. This process was also repeated three times. The samples were dried in an oven at a constant temperature of 60°C. Nanotubes were prepared on the 3D-printed titanium alloy scaffolds by anodic oxidation [31]. The printed porous titanium alloy scaffold was used as the anode while a platinum plate (0.5 mm × $0.5 \, \text{mm} \times 0.1 \, \text{mm}$) was used as the cathode, and the distance between the two electrodes was set to 20 mm. Ethylene glycol solution containing 0.5 wt% NH₄F and 10 vol% deionized water was selected as the electrolyte. In order to observe the effect of anodic oxidation voltage and oxidation time on the nanotube morphology, we obtained three groups of data by setting the voltage to 50, 60, and 70 V, respectively, and the anodic oxidation time to 1h at room temperature and collected another three groups of data by maintaining the voltage at 60 V and setting the anodic oxidation time to 15 min, 30 min, and 1 h, respectively. Three scaffolds of each different type are used in this research to mitigate errors. Finally, all the prepared porous scaffolds were put into a muffle furnace for 2 h of heat treatment to eliminate internal stress and enhance the bonding force between nanotubes and their substrate.

Due to the influence of liquid flow on the diffusion of ions, the anodization within the pores of a porous scaffold may be slower than the external contact surface of the scaffold. Therefore, in this article, the surface inside the scaffold pores is referred as the "inner surface," while the externally accessible surface is referred as the "outer surface." The microscopic structure of the inner and outer surface and the crystallinity of these scaffolds were characterized. The experiments were performed using a SEM (JSE-5900LV, Japan) and the voltage was set to 5.0 kV. The diameter of nanotubes was measured and recorded by the software ImageJ. Then the main components on the sample surface were determined by XRD after 1 h of anodic oxidation at the voltage of 60 V [32].

4 — Shiqi Fan et al. DE GRUYTER

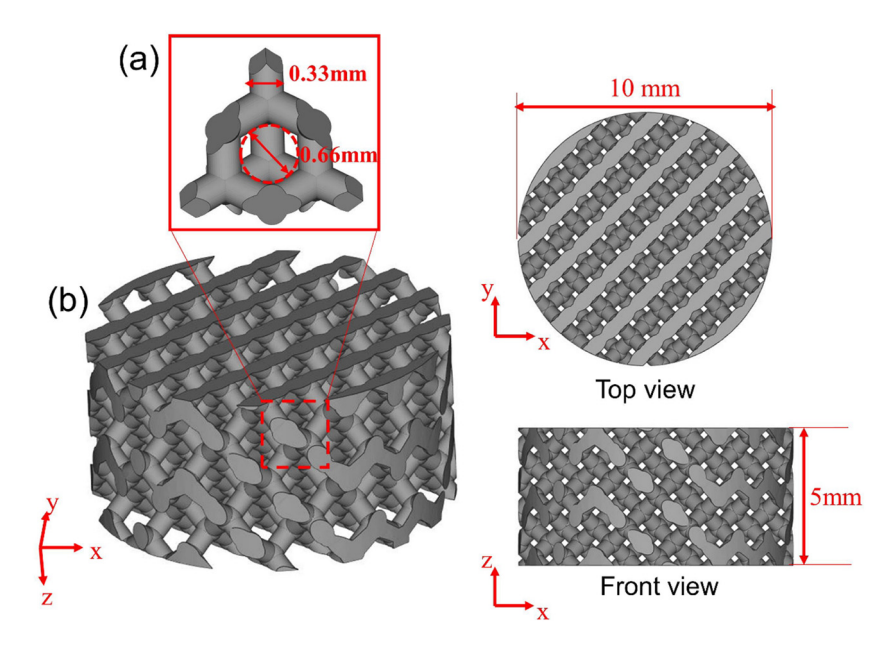


Figure 2: Modeling of scaffold: (a) porous diamond unit, which was used for construction of the main body of porous scaffolds and (b) 3D modeling of the bone tissue engineering scaffold.

2.3 Drug loading treatment of the porous titanium alloy scaffolds

After 1 h of anodic oxidation at the voltage of 60 V under an aseptic condition away from light, the heat-treated scaffolds were immersed into 1 mg·mL⁻¹ MH solution and kept in the solution for 2 h. These scaffolds were taken out of the solution and the coating surfaces were quickly washed with phosphate-buffered saline (PBS) solution to remove the residual drug outside the nanotubes. PLGA was then used to control the drug release rate. PLGA solution of 10 µL with a concentration of 10 mg·mL⁻¹ was added to the surface of the scaffold. After the solution was immersed in the hole of the scaffold, it was put into a drying oven to dry. The process was repeated four times. The scaffolds were put into a hot air oven at the interval between the coatings and then dried. Four specimens of each type of scaffold were used to mitigate test errors. Spectrophotometry was adopted to measure the drug release rate of these scaffolds. After the completion of the preparation experiment, each sample was immersed in 5 mL of PBS solution (0.01 M, pH 7.4) at 37°C. About 3 mL of the solution was replaced after every 5 h and supplemented with same volume of PBS. Three repeated samples were recorded at each time point to learn about the experiment results more accurately. The amount of MH released from the nanotubes was measured by UV-vis spectrophotometer at 360 nm.

2.4 Cytotoxicity test

The experiments were performed using MC3T3-E1 preosteoblastic cells, and the experiments were divided into three groups, each group includes five samples to mitigate errors, which is named as: scaffolds only treated by anodic oxidation (blank), scaffolds loaded with MH, and scaffolds loaded with MH and coated with PLGA (MH/PLGA), MC3T3-E1 cells were seeded in 24-well plates at a density of 4×10^4 cells/scaffold in α-MEM medium (Hyclone, USA) containing 1% penicillin/streptomycin (Hyclone, USA). The cells were cultured under 5% CO2 at 37°C, and the culture medium was changed every other day. After 1, 4, and 7 days of culture, cells were visualized by laser scanning confocal microscopy (Zeiss, SM 800, Germany) using fluorescein diacetate (Sigma), rhodamine phalloidin (Sigma) and 4',6-diamino-2-phenylindole (Sigma) as fluorescent dyes. Meanwhile, cell counting kit-8 (CCK-8; Beyotime, Shanghai) was used for cell counting.

2.5 Anti-infection function test

The inhibitory effect of different samples on gram-positive microorganisms (*Staphylococcus aureus*) was detected by zone of inhibition (ZI). First, the samples were divided into two groups: scaffolds loaded with drug (MH) and scaffolds loaded with MH and then coated with PLGA (MH/PLGA). Three scaffolds from each group were placed in normal

saline and immersed for 3 days. Three scaffolds in each group were without immersion. The immersed scaffolds were rinsed with PBS once before the experiment and dried in a vacuum drying oven. A total of 12 scaffolds were used for subsequent experiments. These 12 samples were placed on LB solid agar Petri dishes containing approximately 10⁴ CFU *S. aureus* per plate so that the coated side of the material was in contact with the inoculated agar. Then, incubation was performed at 37°C for 24 h, and finally a zone was formed as an indicator of anti-infection activity. We conducted ZI statistical analysis using the software ImageJ.

2.6 Statistical analysis

All experimental data expressed as mean \pm standard were calculated based on at least three independent experiments. Statistical analyses were carried out using OriginPro 2022 (OriginLab Corporation, USA). Data were analyzed using GraphPad Prism software (GraphPad Software Inc.) by Student's *t*-test (unpaired and two-tailed), one-way or two-way analysis of variance (ANOVA), followed by Tukey *post-hoc* test. Statistical differences were shown with three significance levels: *p < 0.05, **p < 0.01, and **** p < 0.001.

3 Results and discussion

3.1 Microstructures and the surface characteristics of the porous scaffolds

Refer Figure 3(a) for the particle size of titanium powder used for printing and see Figure 3(b) for the appearance

and dimensions of the finished scaffold. We observed a high degree of sphericity from the spherical powder, with the particle size roughly ranging from 15 to 45 μm . SEM images of lower magnification before and after pickling are shown in Figure 4. It can be observed that scaffold surface is smooth after pickling because the pickling process has removed the residual titanium powder particles that were left by the printing process and had not been fully melted. The residual titanium powder particles may cause harm to the human body, and the pickling process helps improve the scaffold surface quality [33].

When conducting experiments at different anodic oxidation voltages, we observed significant differences in the results, as shown in Figure 5. When the voltage is 50, 60, and 70 V, the diameter of nanotubes is 102, 128, and 152 nm after anodic oxidation for 1h, and the diameter of nanotubes increases with the rising anodic oxidation voltage. The corresponding semi-quantitative results showed significant differences between the groups. The above results indicate that the diameter of nanotubes generated by anodic oxidation is positively correlated with the applied voltage, and can be precisely controlled by regulating the anodic oxidation voltage [34-36]. As shown in Figure 6, we can observe that holes begin to appear on the scaffold surface after the scaffold is anodized for 15 min at the voltage of 60 V. A dense non-conductive oxide layer is generated on the scaffold surface due to oxidation reactions after anodic oxidation starts. With the continuous oxidation reaction, the oxide layer on the metal surface is gradually thickened, thus blocking current flow and slowing down the thickening process of oxide layer. Since Al and V exist in the alloy, the local electrical field density is not uniform and fluorine ions were gathered at the location with large electric field, which is helpful for the chemical dissolution of TiO2. Then holes are formed on the oxide layer through dissolution. After 30 min

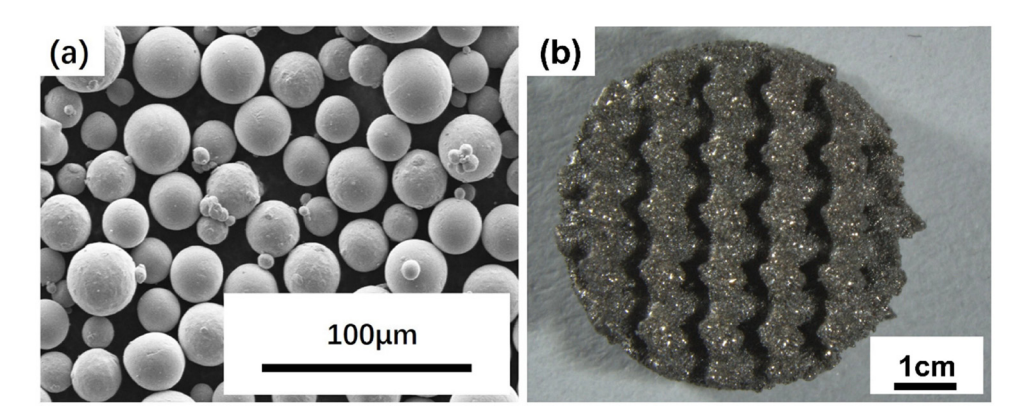


Figure 3: Raw materials and printing scaffold: (a) SEM image of titanium powders used for 3D printed and (b) appearance and dimensions of the obtained 3D printed scaffold.

6 — Shiqi Fan et al. DE GRUYTER

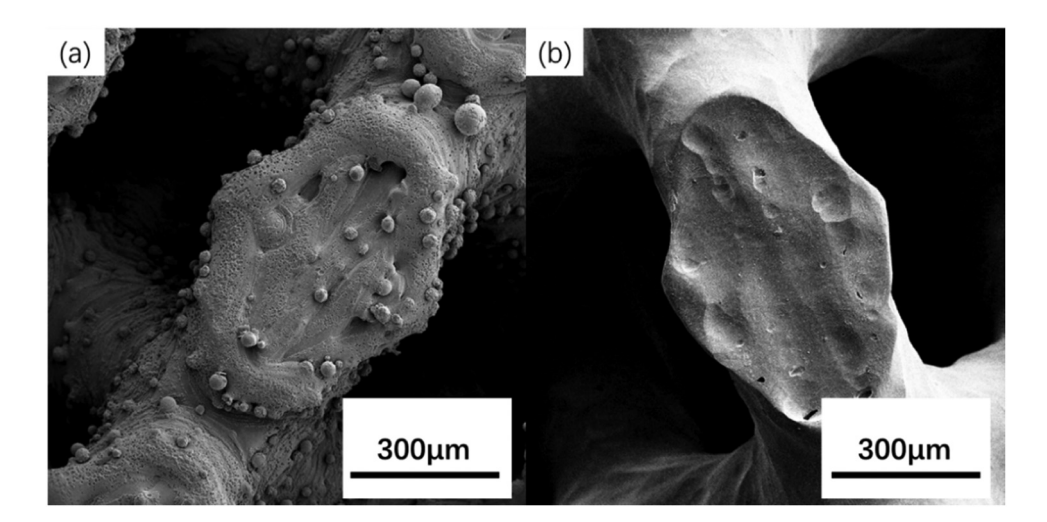


Figure 4: SEM images of scaffolds before and after pickling: (a) appearance of the surface microstructures of the 3D printed scaffold before acid pickling, (b) appearance of the surface microstructures of the 3D printed scaffold after acid pickling, which shows a smooth surface and no residual powder remained on the surface of the scaffold.

of anodic oxidation, we can observe that the outline of nanotubes is gradually formed. After all, the barrier layer at the pit bottom becomes thinner, the electric field density increases and more fluorine ions are accumulated. The accumulation further accelerates the dissolution rate of TiO_2 , and small holes gradually grow into small pores. Unoxidized conductive titanium covered with a thick non-conductive oxide layer can be observed from the

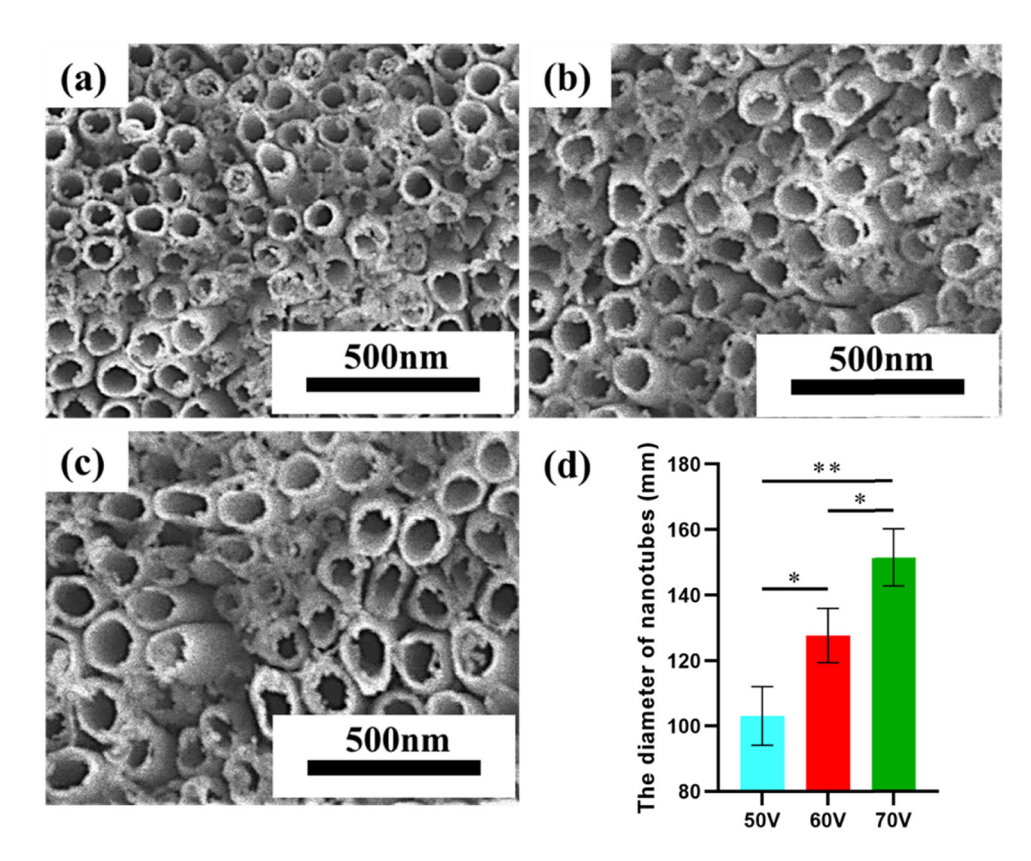


Figure 5: SEM images of nanotubes generated after 1 h of anodization at different voltage levels: (a) 50 V, (b) 60 V, and (c) 70 V. (d) Semi-quantitative results of the diameter of nanotubes. (Two-tailed *t*-test or one-way ANOVA with Tukey, *p < 0.05, **p < 0.01, and ***p < 0.001, error bars represent SD, $n \ge 3$ independent experiments).

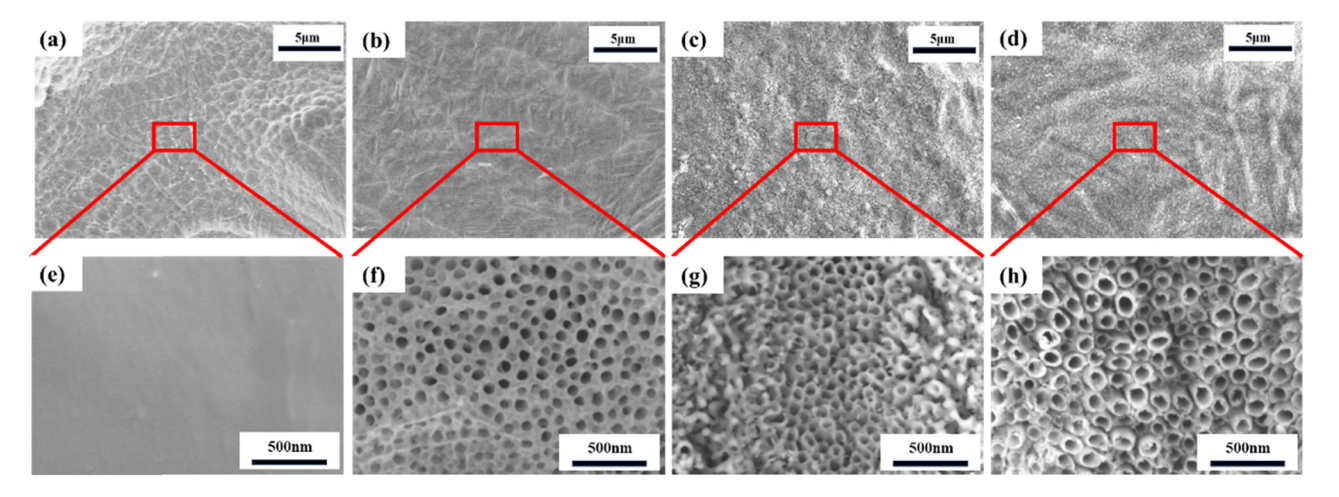


Figure 6: Morphology of nanotubes formed after anodization at a voltage of 60 V for varying durations: (a) low-magnification appearance of unanodized sample, (b) low-magnification appearance after 15 min of anodic oxidation, (c) low-magnification appearance after 30 min of anodic oxidation, (d) low-magnification appearance after 1h of anodic oxidation, (e) micro-surface morphology of unanodized sample, (f) micro-surface morphology after 15 min of anodic oxidation, (g) micro-surface morphology after 30 min of anodic oxidation, and (h) micro-surface morphology after 1h of anodic oxidation.

pore wall region. As the pores grow, these regions protrude, and the electric field density increases greatly due to the underlying conductive titanium. This effect accelerates the chemical dissolution. Since the non-conductive layer near the holes is thicker than that in the relatively distant regions, the dissolution rate is higher at the more distant locations. After 1 h of anodic oxidation, we finally observed the nanotubes with a good morphology, indicating a balance between the chemical dissolution at the bottom of nanotubes and the chemical solution at the mouth of nanotubes. Under such circumstance, the length of nanotubes stops increasing. These experimental results show that anodic oxidation voltage and anodic oxidation time have a significant effect on the growth and morphology of nanotubes, which provides a good condition for the subsequent drug loading of these scaffolds. Due to the formation of nanotubes, the scaffold surface becomes rougher, which significantly improves the surface roughness of the scaffolds. The surface with higher roughness shows better cell adhesions compared to smoother surface [37]. Moreover, rough surfaces can reduce the relative movement between the material and surrounding tissue, thereby relieving friction and irritation, reducing the inflammatory response caused by the material, improving the wetting properties of the material and making it easier to contact with biological fluids. A rough surface is important for such applications as medical devices, biosensors, and drug delivery systems because it can increase the interfacial area between materials and biological fluids to increase the efficiency of adhesion [36,38].

The scaffold after 1 h of anodic oxidation at 60 V was taken as a sample and the surface properties of this scaffold were tested. The XRD pattern shows that differently from the scaffolds not treated through anodic oxidation, the surface of the scaffolds after anodic oxidation has generated TiO₂ nanotubes with anatase structure, as shown in Figure 7. Titanium dioxide is a naturally occurring oxide of titanium and is commonly found in three main crystal structures: rutile, anatase, and brookite. The anatase structure is one of these crystal structures, and it has distinct physical and chemical properties. Anatase is characterized by tetragonal crystal symmetry, meaning its unit cell has a fourfold rotational symmetry axis. The crystal lattice arrangement in anatase is different from that of rutile and brookite. The nanotubes with anatase structure are proved to have better

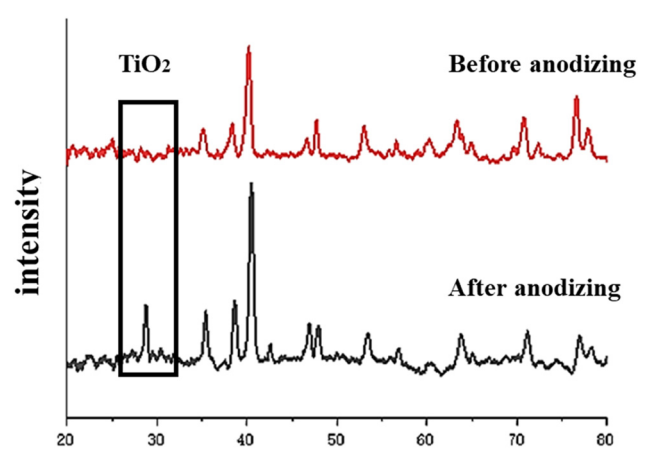


Figure 7: XRD pattern of the scaffold before and after anodic oxidation.

8 — Shigi Fan et al. DE GRUYTER

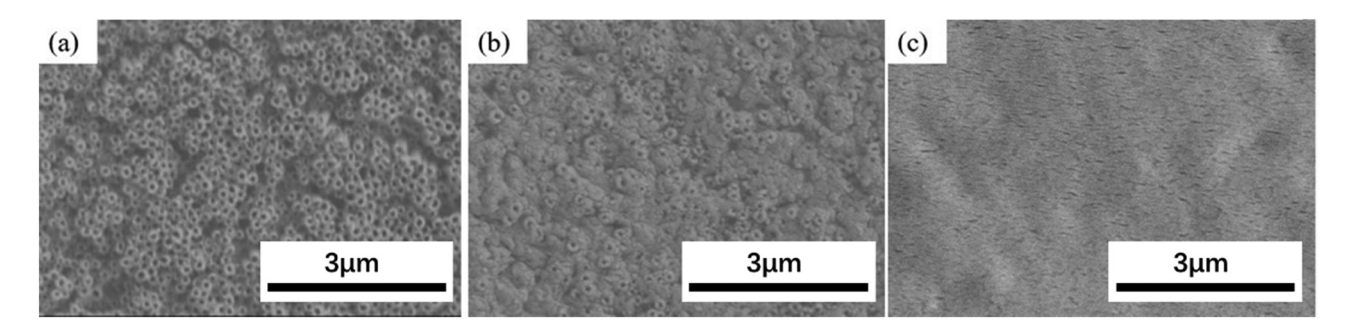


Figure 8: SEM images of the scaffold surface morphologies: (a) scaffolds are not loaded with drug, (b) scaffolds are loaded with MH, and (c) scaffold are loaded with MH and coated with PLGA.

physical and chemical properties and contribute more to the osseointegration of orthopedic scaffolds [39,40].

3.2 Drug loading results of the scaffolds

After the scaffolds were finished and loaded with MH, the top view of the nanotubes and the morphological changes before and after drug loading were observed by means of SEM. As shown in Figure 8(a), the nanotubes before drug loading are composed of densely arranged tubular structures, and the top of them is in an open state, presenting a highly ordered layered structure. The morphology of the nanotubes after immersed in MH solution is shown in Figure 8(b) and the gaps between nanotubes are filled with MH. In order to slow down the drug release, the nanotubes loaded with MH are further covered with PLGA. The top morphology of the composite coating (nanotube/MH/ PLGA) is shown in Figure 8(c). The surface is smooth and glossy and we cannot observe any tubular structure. Further studies have verified the successful deposition of MH in the nanotubes [41].

Drug release kinetics is one of the important factors to control the therapeutic effects and side effects of drugs. The in vitro drug release behavior of the scaffolds only loaded with MH and of the scaffolds loaded with MH and then coated with PLGA was evaluated during the experiments. As shown in Figure 9, the experimental results show that the two types of scaffolds have different behaviors in terms of drug release. For the scaffolds only loaded with MH, the burst drug release behavior appeared within 25 h, and the drug release rate increased rapidly and then gradually stabilized after the burst drug release. For the scaffolds loaded with MH and then coated with PLGA, the initial release rate was lower, the release amount in 24 h was 48% of that from the scaffolds not coated with PLGA and only a small amount of drug was released. There was a significant difference in drug release between the two scaffolds at each time point. Then the release was steadily accelerated and tended to be consistent at last, with no significant difference in drug release between the two scaffolds at each time point. These results indicate that the scaffolds coated with PLGA on the surface can effectively reduce drug release rate.

3.3 Cytotoxicity test of the porous titanium alloy scaffolds

CCK-8 experimental results are shown in Figure 10. In the experiment, the growth and survival of MC3T3-E1 preosteo-blastic cells were affected by different scaffold materials. First of all, in the blank scaffolds, the number of cells showed a stable growth trend, indicating that the scaffold material has no significant effect on cell growth and survival. However, massive cell deaths occurred on the first day and cells increased steadily on the fourth and seventh day on the scaffolds only loaded with MH. However, they were significantly different from the blank scaffolds at the same period. Cytotoxicity was caused by the burst release

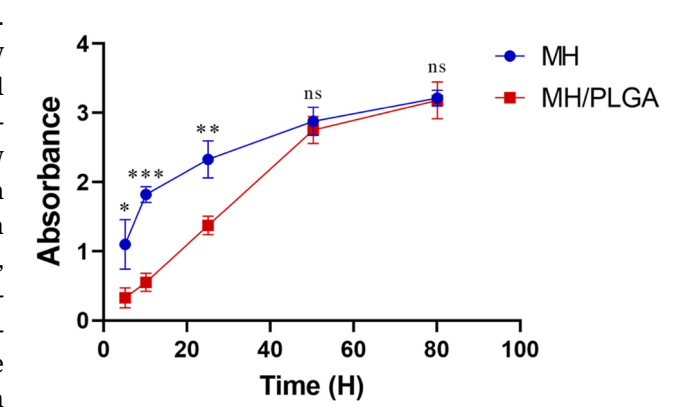


Figure 9: Drug release curve of the porous titanium alloy scaffolds. (Two-tailed *t*-test or one-way ANOVA with Tukey, *p < 0.05, **p < 0.01, and ***p < 0.001, error bars represent SD, $n \ge 3$ independent experiments.).

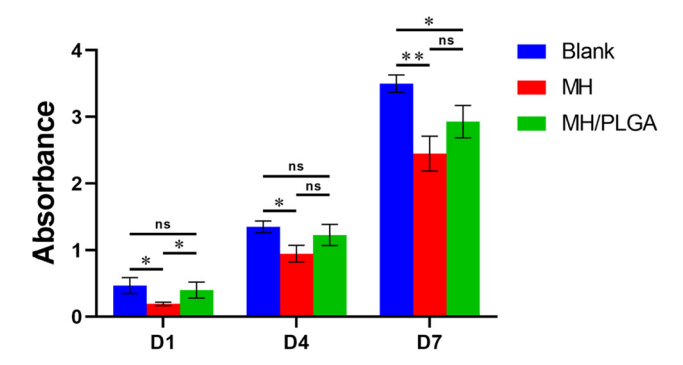


Figure 10: Cell CCK-8 results of different porous titanium alloy scaffolds. (Two-tailed t-test or one-way ANOVA with Tukey, *p < 0.05, **p < 0.01, and ***p < 0.001, error bars represent SD, $n \ge 3$ independent experiments).

of MH, resulting in massive cell death especially in the initial culture phase. The cell growth on the scaffolds coated with PLGA (MH/PLGA) was slight on the first day and many dead cells were detected on the fourth day. This situation may be caused by the harmful substances released

by the degradation of PLGA and the substances produce an adverse effect to cells. However, the number of cells increased steadily on the seventh day, indicating that the substances from the degradation of PLGA had been fully released or the cells had gradually adapted to the environment and begun to grow again. A similar conclusion was obtained from the results of a cell survival experiment, as shown in Figure 11. In the experiment with blank scaffolds, the number of cells increased gradually, and almost no dead cells appeared. In the experiment on the scaffolds only loaded with MH, the fact that there were fewer viable cells than the other two groups were observed on the first day. This fact resulted from the toxicity caused by MH in the scaffolds. In the subsequent experiments, we observed an increasing number of cells since the fourth day, indicating that cells could still continue to proliferate on the scaffolds only loaded with drug. Although fewer viable cells were observed on the first day, the death rate of cells decreased gradually and the number of cells was gradually restored to a normal level in the subsequent experiments. For the

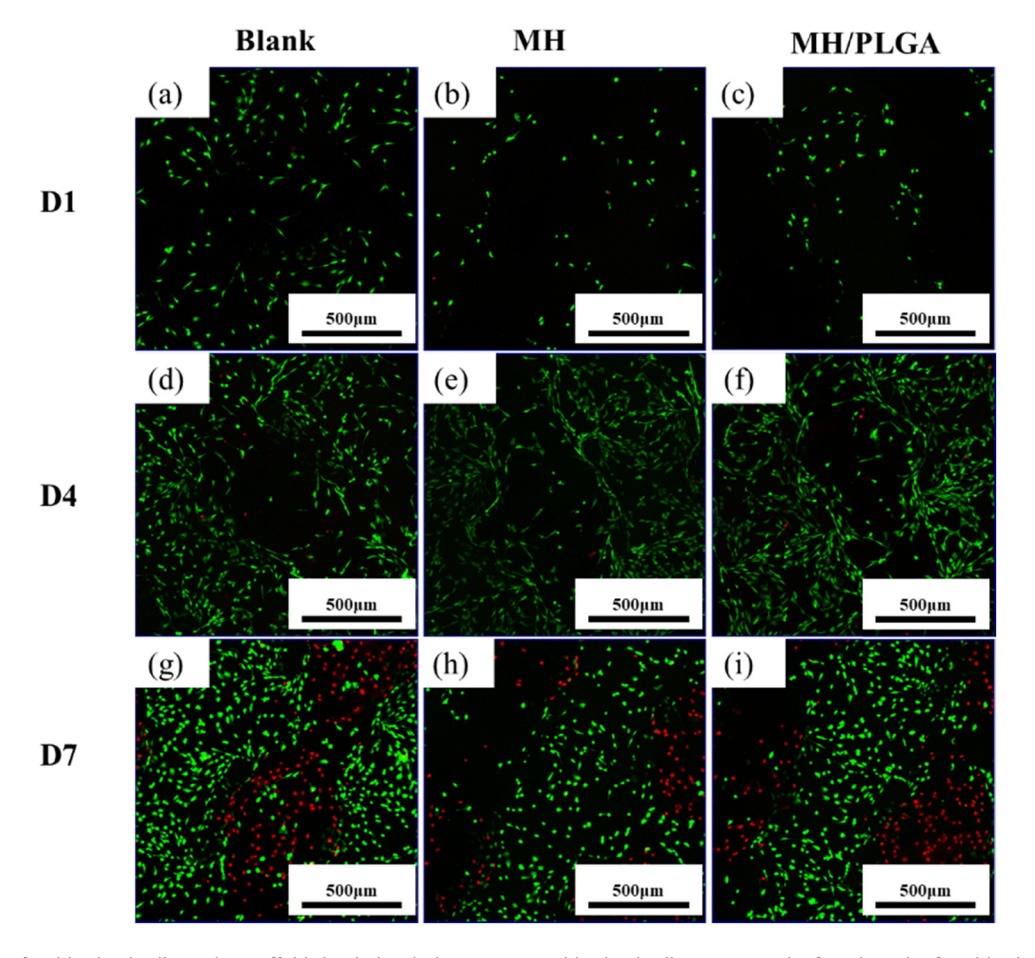


Figure 11: Test of viable/dead cells on the scaffolds loaded with drug: (a)–(c) viable/dead cell staining on the first day, (d)–(f) viable/dead cell staining on the fourth day, and (g)–(i) viable/dead cell staining on the seventh day. The red dots are the dead cells and the green dots are the live cells.

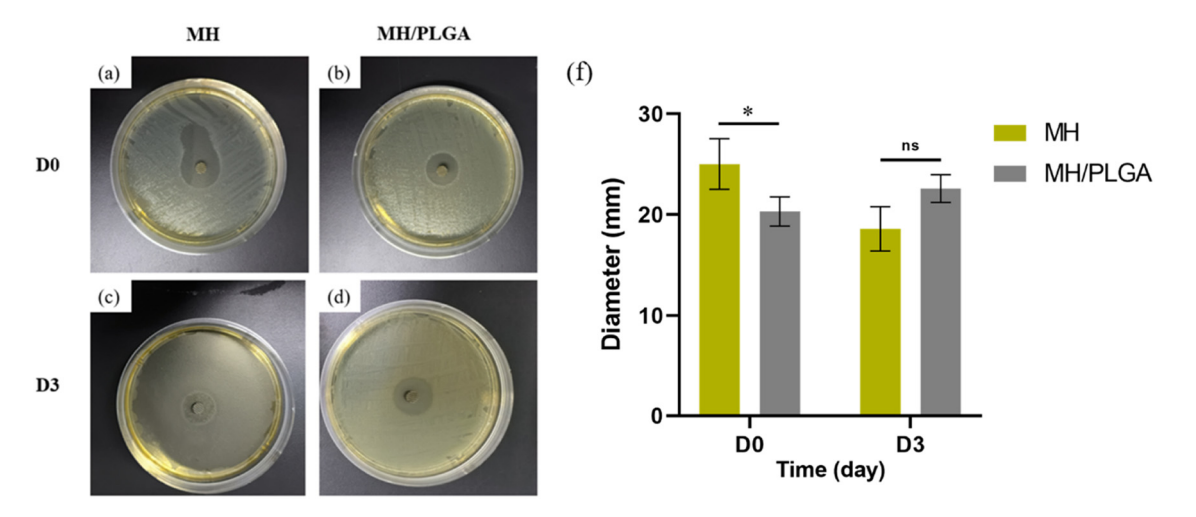


Figure 12: Anti-infection test results: (a) and (b) ZI of the two types of drug-loaded scaffolds before immersion, (c) and (d) ZI of the two types of drug-loaded scaffolds after immersion for 3 days, and (e) semi-quantitative results of ZI diameters. (Two-tailed *t*-test or one-way ANOVA with Tukey, *p < 0.05, **p < 0.01, and ***p < 0.001, error bars represent SD, p ≥ 3 independent experiments).

scaffolds coated with PLGA, fewer cells died on the first day than for the scaffolds only loaded with drug. This is because the release of PLGA is a slow process and will not cause severe damage to cells. However, an increasing number of dead cells was observed on the fourth day, indicating that the degradation of PLGA released some loaded drugs and produced some adverse effects on the cells. These effects are within an acceptable range. According to the relevant results, the scaffolds only loaded with MH can significantly inhibit cell proliferation at beginning, but the cells are still viable and will proliferate later. Differently from the scaffolds only loaded with MH, the scaffolds loaded with MH and coated with PLGA can slow down the drug release to a certain extent, thus achieving sustained drug release and reducing the number of cell deaths in the early phase of cell culture. Certainly, the presence of PLGA on the surface of the scaffold also alters the mechanical properties of the scaffold's surface and has a certain impact on cell adhesion. These findings confirmed some previous literature [42]. Considering the above, PLGA has an excellent effect in slowing down drug release. It is expected to apply PLGA to the design of drug delivery systems.

3.4 Anti-infection function test of the scaffolds

The anti-infection test results are shown in Figure 12. According to the results, both drug-loaded scaffolds have anti-infection effects with obvious ZI before immersion and the ZI diameter of MH scaffolds is greater than that of MH/PLGA scaffolds. The corresponding semi-quantitative

results showed significant differences between the two groups. ZI still appears on MH scaffolds after immersion. However, the ZI is smaller and shows a lighter color than before. It indicates that the release of MH is affected by immersion. The loaded drug is released quickly, resulting in a rapid decline in its anti-infection effect. Only a small amount of drug solution still exists on the scaffold, showing a very weak anti-infection effect. The corresponding semi-quantitative results showed no significant difference between the two groups. Before immersion, the MH/PLGA scaffolds have an excellent anti-infection effect. After immersion, the anti-infection effect can be preserved, indicating that the MH/PLGA scaffolds have a certain sustained good anti-infection activity and proving that the coating of PLGA can delay the release of MH and maintain its anti-infection effect.

4 Conclusions

In this study, it was verified that anodic oxidation voltage and anodic oxidation time could achieve a microscopic regulation over the morphology of nanotubes. The experimental results showed that the diameter of nanotubes was positively correlated with anodic oxidation voltage and times, the nanotubes with good morphology of about 128 nm diameter can be obtained after 1 h of anodic oxidation at 60 V. These nanotubes showed a good drug loading potential for anti-infection function design. We proposed an effective drug loading method to control the slow release behavior of MH loaded on nanotubes through PLGA coatings. According to the results of SEM and drug

release experiments, the scaffolds loaded with MH and coated with PLGA were successfully prepared and showed good sustained drug release curve. As demonstrated by the subsequent in vitro cell experiments, PLGA coating delayed the drug release and effectively reduced the cytotoxicity. The anti-infection test results showed that the drug-loaded scaffolds with PLGA coating provided a sustained antiinfection biofunction. This drug-loading scaffold can be customized on an individual basis to meet the diverse needs of different patients, and the drug-loading coating is also relatively easy to implement, which proves beneficial for practical applications. These results provided a novel strategy to design the anti-infection functions of 3D printed titanium alloy bone tissue engineering scaffolds.

Funding information: This work was partially supported by the National Key Research and Development Program of China (2023YFC2411300, 2019YFA0110600). Science and Technology Project of Tibet Autonomous Region (XZ202202YD0013C, XZ202102YD0026C). Sichuan Science and Technology Program (2021YJ0135, 2023YFQ0053, 2022YFS0197). Innovation research projects of Sichuan University (2023SCUH0015, 0040206107025).

Author contributions: Shigi Fan: conceptualization, investigation, writing - review and editing. Zhen Tan: conceptualization, investigation, writing – review and editing. Zhiyu Peng: investigation, methodology. Shilei Li: data curation, formal analysis. Haoyuan Lei: methodology, software. Yuxiang Qin: supervision, project administration. Hongyuan Fan: supervision, project administration. Yuanhua Lin: supervision, project administration. Changchun Zhou: data curation, resources, supervision, project administration. All authors have accepted responsibility for the entire content of this manuscript and approved its submission.

Conflict of interest: The authors state no conflict of interest.

References

- Zhang, S., Q. Wei, L. Cheng, S. Li, and Y. Shi. Effects of scan line [1] spacing on pore characteristics and mechanical properties of porous Ti6Al4V implants fabricated by selective laser melting. Materials & Design, Vol. 63, 2014, pp. 185-193.
- Vetrik, M., M. Parizek, D. Hadraba, O. Kukackova, J. Brus, H. Hlidkova, et al. Porous heat-treated polyacrylonitrile scaffolds for bone tissue engineering. ACS Applied Materials & Interfaces, Vol. 10, 2018, pp. 8496-8506.
- Yao, Q., Y. Liu, B. Selvaratnam, R. T. Koodali, and H. Sun. Mesoporous silicate nanoparticles/3D nanofibrous scaffold-

- mediated dual-drug delivery for bone tissue engineering. Journal of Controlled Release, Vol. 279, 2018, pp. 69-78.
- [4] Zhang, J., D. Xiao, X. He, F. Shi, P. Luo, W. Zhi, et al. A novel porous bioceramic scaffold by accumulating hydroxyapatite spheres for large bone tissue engineering. III: characterization of porous structure. Materials Science & Engineering, C: Materials for Biological Applications, Vol. 89, 2018, pp. 223-229.
- Zhou, C., X. Ye, Y. Fan, L. Ma, Y. Tan, F. Qing, et al. Biomimetic [5] fabrication of a three-level hierarchical calcium phosphate/collagen/hydroxyapatite scaffold for bone tissue engineering. Biofabrication, Vol. 6, 2014, id. 035013.
- Yan, Y., Y. Kang, D. Li, K. Yu, T. Xiao, Q. Wang, et al. Microstructure, mechanical properties and corrosion behavior of porous Mg-6 wt% Zn scaffolds for bone tissue engineering. *Journal of Materials* Engineering and Performance, Vol. 27, 2018, pp. 970-984.
- Bartolomeu, F., N. Dourado, F. Pereira, N. Alves, G. Miranda, and [7] F. S. Silva. Additive manufactured porous biomaterials targeting orthopedic implants: a suitable combination of mechanical, physical and topological properties. Materials Science & Engineering, C: Materials for Biological Applications, Vol. 107, 2020, id. 110342.
- Li, H., M. Ramezani, M. Li, C. Ma, and J. Wang. Effect of process [8] parameters on tribological performance of 316L stainless steel parts fabricated by selective laser melting. Manufacturing Letters, Vol. 16, 2018, pp. 36-39.
- Zhang, H., H. Zhu, T. Qi, Z. Hu, and X. Zeng. Selective laser melting of high strength Al-Cu-Mg alloys: processing, microstructure and mechanical properties. Materials Science and Engineering A, Vol. 656, 2016, pp. 47-54.
- Zhang, L., S. Zhang, H. Zhu, Z. Hu, G. Wang, and X. Zeng. Horizontal [10] dimensional accuracy prediction of selective laser melting. Materials & Design, Vol. 160, 2018, pp. 9-20.
- Chen, Q. and G. A. Thouas. Metallic implant biomaterials. Materials Science and Engineering R, Vol. 87, 2015, pp. 1-57.
- [12] Bandyopadhyay, A., A. Shivaram, S. Tarafder, H. Sahasrabudhe, D. Banerjee, and S. Bose. In vivo response of laser processed porous titanium implants for load-bearing implants. Annals of Biomedical Engineering, Vol. 45, 2017, pp. 249–260.
- Pobloth, A. M., S. Checa, H. Razi, A. Petersen, J. C. Weaver, K. Schmidt-Bleek, et al. Mechanobiologically optimized 3D titanium-mesh scaffolds enhance bone regeneration in critical segmental defects in sheep. Science Translational Medicine, Vol. 10, 2018, pp. 1-16.
- Wang, X., S. Xu, S. Zhou, W. Xu, M. Leary, P. Choong, et al. [14] Topological design and additive manufacturing of porous metals for bone scaffolds and orthopaedic implants: a review. Biomaterials, Vol. 83, 2016, pp. 127-141.
- [15] Wu, S., X. Liu, K. W. K. Yeung, C. Liu, and X. Yang. Biomimetic porous scaffolds for bone tissue engineering. Materials Science and Engineering R, Vol. 80, 2014, pp. 1-36.
- Zadpoor, A. A.. Mechanical performance of additively manufactured meta-biomaterials. Acta Biomaterialia, Vol. 85, 2019,
- [17] Yu, M., Y. Wan, B. Ren, H. Wang, X. Zhang, C. Qiu, et al. 3D printed Ti-6Al-4V implant with a micro/nanostructured surface and its cellular responses. ACS Omega, Vol. 5, 2020, pp. 31738-31743.
- Sun, L., J. Xu, Z. Sun, F. Zheng, C. Liu, C. Wang, et al. Decreased porphyromonas gingivalis adhesion and improved biocompatibility on tetracycline-loaded TiO₂ nanotubes: an in vitro study. International Journal of Nanomedicine, Vol. 13, 2018, id. 6769.
- Arenas, M. A., C. Pérez-Jorge, A. Conde, E. Matykina, J. M. Hernández-López, R. Pérez-Tanoira, et al. Doped TiO₂ anodic layers

- of enhanced antibacterial properties. *Colloids and Surfaces B Biointerfaces*, Vol. 105, 2013, pp. 106–112.
- [20] Fu, Y. and A. Mo. A review on the electrochemically self-organized titania nanotube arrays: synthesis, modifications, and biomedical applications. *Nanoscale Research Letters*, Vol. 13, 2018, pp. 1–21.
- [21] Chen, Y., J. Ni, H. Wu, R. Zhang, C. Zhao, W. Chen, et al. Study of cell behaviors on anodized TiO₂ nanotube arrays with coexisting multisize diameters. *Nano-Micro Letter*, Vol. 8, 2016, pp. 61–69.
- [22] Yavari, S. A., J. van der Stok, Y. C. Chai, R. Wauthle, Z. T. Birgani, P. Habibovic, et al. Bone regeneration performance of surface-treated porous titanium. *Biomaterials*, Vol. 35, 2014, pp. 6172–6181.
- [23] Yang, Y., H.-y Ao, S.-b Yang, Y.-g Wang, W.-t Lin, Z.-f Yu, et al. In vivo evaluation of the anti-infection potential of gentamicin-loaded nanotubes on titania implants. *International Journal of Nanomedicine*, Vol. 11, 2016, id. 2223.
- [24] Martins, C., F. Sousa, F. Araújo, and B. Sarmento. Functionalizing PLGA and PLGA derivatives for drug delivery and tissue regeneration applications, advanced healthcare. *Materials*, Vol. 7, 2018, id. 1701035.
- [25] Park, J.-W., J.-U. Hwang, J.-H. Back, S.-W. Jang, H.-J. Kim, P.-S. Kim, et al. High strength PLGA/hydroxyapatite composites with tunable surface structure using PLGA direct grafting method for orthopedic implants. *Composites Part B: Engineering*, Vol. 178, 2019, id. 107449.
- [26] Feng, W., Z. Geng, Z. Li, Z. Cui, S. Zhu, Y. Liang, et al. Controlled release behaviour and antibacterial effects of antibiotic-loaded titania nanotubes. *Materials Science & Engineering, C: Materials for Biological Applications*, Vol. 62, 2016, pp. 105–112.
- [27] Li, Y., Y. Yang, R. Li, X. Tang, D. Guo, and Y. Qin. Enhanced anti-bacterial properties of orthopedic implants by titanium nanotube surface modification: a review of current techniques. *International Journal of Nanomedicine*, Vol. 14, 2019, pp. 7217–7237.
- [28] Wang, Z., C. Wang, C. Li, Y. Qin, L. Zhong, B. Chen, et al. Analysis of factors influencing bone ingrowth into three-dimensional printed porous metal scaffolds: a review. *Journal of Alloys and Compounds*, Vol. 717, 2017, pp. 271–285.
- [29] Lei, H., Z. Zhou, L. Liu, C. Gao, Z. Su, Z. Tan, et al. Icariin-loaded 3D-printed porous Ti6Al4V reconstruction rods for the treatment of necrotic femoral heads. *Acta Biomaterialia*, Vol. 169, 2023, pp. 625–640.
- [30] Song, P., C. Hu, X. Pei, J. Sun, H. Sun, L. Wu, et al. Dual modulation of crystallinity and macro-/microstructures of 3D printed porous titanium implants to enhance stability and osseointegration. *Journal of Materials Chemistry B: Materials for Biology and Medicine*, Vol. 7, 2019, pp. 2865–2877.
- [31] Dong, J., J. Han, X. Ouyang, and W. Gao. How voltage dictates anodic TiO₂ formation. *Scripta Materialia*, Vol. 94, 2015, pp. 32–35.
- [32] Qin, J., D. Yang, S. Maher, L. Lima-Marques, Y. Zhou, Y. Chen, et al. Micro- and nano-structured 3D printed titanium implants with a

- hydroxyapatite coating for improved osseointegration. *Journal of Materials Chemistry B: Materials for Biology and Medicine*, Vol. 6, 2018, pp. 3136–3144.
- [33] Pyka, G., A. Burakowski, G. Kerckhofs, M. Moesen, S. Van Bael, J. Schrooten, et al. Surface modification of Ti6Al4V open porous structures produced by additive manufacturing. *Advanced Engineering Materials*, Vol. 14, 2012, pp. 363–370.
- [34] Fan, S., M. Talha, X. Yu, H. Lei, Y. Tan, H. Zhang, et al. 3D printing of porous Ti6Al4V bone tissue engineering scaffold and surface anodization preparation of nanotubes to enhance its biological property. *Nanotechnology Reviews*, Vol. 12, 2023, id. 20230572.
- [35] Xie, Y., X. Chen, X. Zheng, L. Li, J. Li, Y. Xu, et al. Beta1-integrin/ Hedgehog-Gli1 signaling pathway fuels the diameter-dependent osteoblast differentiation on different TiO₂ nanotubes: the optimaldiameter nanotubes for osteoblast differentiation. *The International Journal of Biochemistry & Cell Biology*, Vol. 137, 2021, id. 106026.
- [36] Gong, Z., Y. Hu, F. Gao, L. Quan, T. Liu, T. Gong, et al. Effects of diameters and crystals of titanium dioxide nanotube arrays on blood compatibility and endothelial cell behaviors. *Colloids and Surfaces B Biointerfaces*, Vol. 184, 2019, id. 110521.
- [37] Deligianni, D. D., N. Katsala, S. Ladas, D. Sotiropoulou, J. Amedee, and Y. Missirlis. Effect of surface roughness of the titanium alloy Ti–6Al–4V on human bone marrow cell response and on protein adsorption. *Biomaterials*, Vol. 22, 2001, pp. 1241–1251.
- [38] Huang, Q., T. A. Elkhooly, X. Liu, R. Zhang, X. Yang, Z. Shen, et al. Effects of hierarchical micro/nano-topographies on the morphology, proliferation and differentiation of osteoblastlike cells. *Colloids and Surfaces B Biointerfaces*, Vol. 145, 2016, pp. 37–45.
- [39] Amin Yavari, S., L. Loozen, F. L. Paganelli, S. Bakhshandeh, K. Lietaert, J. A. Groot, et al. Antibacterial behavior of additively manufactured porous titanium with nanotubular surfaces releasing silver ions. ACS Applied Materials & Interfaces, Vol. 8, 2016, pp. 17080–17089.
- [40] Decha-umphai, D., H.-T. Chunate, T. Phetrattanarangsi, T. Boonchuduang, M. Choosri, C. Puncreobutr, et al. Effects of postprocessing on microstructure and adhesion strength of TiO₂ nanotubes on 3D-printed Ti-6Al-4V alloy. Surface and Coatings Technology, Vol. 421, 2021, id. 127431.
- [41] Liang, Y., Z. Cui, S. Zhu, and X. Yang. Characterization of selforganized TiO₂ nanotubes on Ti–4Zr–22Nb–2Sn alloys and the application in drug delivery system. *Journal of Materials Science: Materials in Medicine*, Vol. 22, 2011, pp. 461–467.
- [42] Bontempi, M., G. Marchiori, M. Petretta, R. Capozza, B. Grigolo, G. Giavaresi, et al. Nanomechanical mapping of three dimensionally printed poly-ε-caprolactone single microfibers at the cell scale for bone tissue engineering applications. *Biomimetics*, Vol. 8, 2023, id. 617.